Electric vehicle battery charging algorithm using PMSM windings and an inverter as an active rectifier

Zaja, Mario; Oprea, Matei-Ion; Suárez, Carlos Gómez; Mathe, Laszlo

Published in:
Proceedings of the 2014 IEEE Vehicle Power and Propulsion Conference (VPPC)

DOI (link to publication from Publisher):
10.1109/VPPC.2014.7007057

Publication date:
2014

Document Version
Early version, also known as pre-print

Electric vehicle battery charging algorithm using PMSM windings and an inverter as an active rectifier

Mario Zaja
Department of Energy Technology
Aalborg University
Aalborg, Denmark
mzaja13@student.aau.dk

Matei Oprea
Department of Energy Technology
Aalborg University
Aalborg, Denmark
moprea13@student.aau.dk

Carlos Gómez Suárez
Department of Energy Technology
Aalborg University
Aalborg, Denmark
cgomez14@student.aau.dk

Laszlo Mathe
Department of Energy Technology
Aalborg University
Aalborg, Denmark
lam@et.aau.dk

***Abstract* - A major setback for large scale electric vehicle market expansion compared to their internal combustion competitors consists in their high price and low driving range. One way of reducing the cost, dimensions and mass of electric vehicles is to eliminate the dedicated AC/DC converter used for battery charging. Alternatively, charging could be done using the motor windings as grid side inductors and controlling the inverter to operate as an active boost rectifier. The challenge in this approach is the unequal phase inductances which depend on the rotor position. Another problem appears when the battery gets discharged below the peak of the grid voltage, typically if the vehicle has not been used for a longer period of time. To avoid high currents that could damage the battery, a voltage suppression mode is introduced for safe depleted battery charging. This paper proposes and analyzes an integrated charger control algorithm to charge the battery through a permanent magnet synchronous machine (PMSM) windings.**

Keywords - electric vehicle, battery charging, space vector modulation, asymmetric, unbalanced, active rectifier, voltage suppression

I. INTRODUCTION

Electric vehicles are one of the most promising solutions to reduce the nowadays' excessive greenhouse gasses emission. Even though many car manufacturers have released their respective electric models over the last couple of years, pure vehicle production is not enough to achieve the goal. Personal electric vehicles have to become widely used among the community to have a significant environmental impact. According to [1], number one barrier for electric car penetration is their cost, while the driving range is the second. The problems are very closely related as batteries account for a significant portion of the vehicle cost and mass [2]. Therefore, any savings regarding cost and weight in the electric vehicle design are very important.

In this paper the use of a built-in inverter and motor windings as an active rectifier to charge the vehicle batteries is analyzed, eliminating the need for an additional AC/DC converter, reducing the mass, size and cost. The difficulty of this approach in comparison to conventional 3 phase rectifiers is the unequal phase inductances dependent on the rotor position. In addition, the presence of electric current in stator windings will cause the rotor to vibrate, alternating its position and introducing non-linearities to the system. Moreover, the boost rectifier cannot operate below the diode bridge rectifier voltage, which becomes an issue in case the vehicle has not been used for a longer period of time and the battery voltage has dropped below that level due to self-discharge. In that case high charging currents may appear and damage the battery.

Previous work [3] - [4] conducted in this field shows that this approach is feasible and both the high power factor and low total harmonic distortion (THD) values can be achieved by regulating each of the phases independently. This paper proposes a way of controlling the power converter using space vector modulation (SVM). Additional control blocks feature generic algorithms independent of machine parameters. A novelty introduced is the voltage supression mode for safe charging of depleted batteries and experimental verification of the solution.

II. SYSTEM LAYOUT

The basic system layout is shown in Fig. 1. Main components of this system are: permanent magnet synchronous machine (PMSM), power converter, battery and a converter control system.

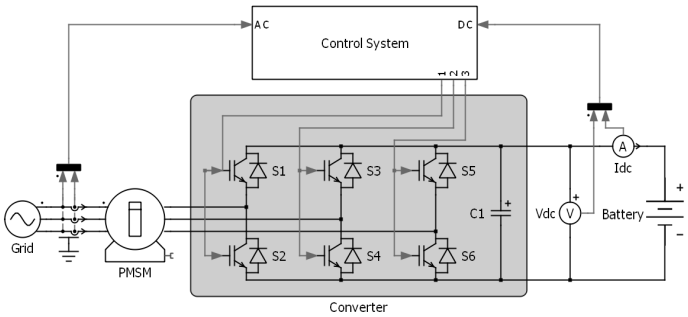

Fig. 1 - Standard active boost rectifier scheme with motor windings used as boost inductors and an inverter to control the battery charging current

Connection to a three phase outlet is established through the machine windings. Winding inductances smoothen the input current waveform and are used for the boost operation mode. A two level power converter is connected to the control system which generates the gate signals for the converter. DC link capacitor is used to stabilize the DC link voltage. Voltage and current measurements are taken at the grid outlet and battery terminals and fed into the control system to form feedback loops.

A. Permanent magnet synchronous machine

Due to their high power-to-mass ratio, PMSMs are widely used in electro mobility sector. Another advantage of using a synchronous machine over asynchronous in charging applications is its inability to rotate when directly connected to the grid from stationary state. This is very important as the motor might be connected directly to the mechanical system and in case of an asynchronous machine, the rotating magnetic field created by the grid voltage would force the machine to rotate and develop torque, causing the vehicle to move and requiring significant mechanical braking power to keep the rotor in place. In case of a PMSM, establishing a direct connection to the grid will cause the rotor to tremble but will not develop any significant torque or rotate the machine, so external mechanical blockade of the rotor is not required.

In some cases the stator inductances of a PMSM depend on the rotor position. Neglecting the higher order terms, this can be well approximated and represented by the equations (1) - (5).

$$L_{mean} = \frac{L_d + L_q}{2} \tag{1}$$

$$L_{var} = \frac{L_d - L_q}{2} \tag{2}$$

$$L_a = L_{mean} + L_{var} \cos\left(p \cdot \theta_r\right) \tag{3}$$

$$L_b = L_{mean} + L_{var} \cos\left(p \cdot \theta_r - 120°\right) \tag{4}$$

$$L_c = L_{mean} + L_{var} \cos\left(p \cdot \theta_r + 120°\right) \tag{5}$$

From the equations (3) - (5) it is visible that all three of the inductances will never have the same value at any given rotor position unless $L_d = L_q$. This will cause unequal phase currents through the machine windings as the grid acts like a voltage source. An example is shown in Fig. 2. Phase currents are transformed into the α-β reference frame and plotted in the XY plane. In a balanced system, the current vector's trajectory is a circle with the center in the origin. A disbalance in the phase inductances causes the trajectory to change shape to an oval as the phase current amplitudes are different.

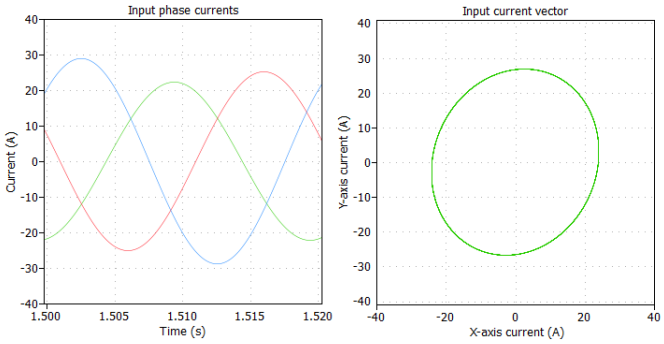

Fig. 2 - Input phase currents for the disbalanced system

As the machine can be stopped at any time and any rotor position, it is important to configure the system to work in the worst case scenario, which is the point of greatest disbalance. To measure the system disbalance and determine the least feasible rotor position, an imaginary inductance vector $\overrightarrow{L_0}$ is introduced and defined as

$$\overrightarrow{L_0} = L_a \cdot e^{j0} + L_b \cdot e^{j\frac{2\pi}{3}} + L_c \cdot e^{-j\frac{2\pi}{3}} \tag{6}$$

Vector $\overrightarrow{L_0}$ represents the inductance bias. In other words, it points in the direction in which the difference between the actual and mean inductance value is the highest, while its magnitude represents the amount of system disbalance. In perfectly balanced systems $\overrightarrow{L_0} = 0$. From a physical viewpoint, $\overrightarrow{L_0}$ points in the direction in which the current vector has the smallest amplitude.

To determine the rotor position of highest disbalance, an absolute value of $\overrightarrow{L_0}$ is calculated. Placing the equations (1) - (5) into (6) and taking the absolute value yields

$$\left|\overrightarrow{L_0}\right| = \frac{3}{4}(L_d - L_q) \tag{7}$$

Equation (7) shows that the magnitude of inductance disbalance is constant and independent of the rotor position. Therefore, any rotor position will cause the same amount of disbalance.

During the charging operation rotor will tremble, causing small changes in phase inductances. These small changes will introduce non-linearities to system as the parameters become time dependent. As a result, changes in voltage drop across the inductances will occur, as described by

$$v_L = \frac{d}{dt}(L \cdot i_L) = i_L \cdot \frac{dL}{dt} + L \cdot \frac{di_L}{dt} \tag{8}$$

For the downscale lab model featuring a 2.2 kW PMSM rotor vibrations have been measured. The machine parameters are as follows: $L_d = 41.59\ mH, L_q = 57.06\ mH, R = 3.30\ \Omega$. The response is shown in Fig. 3.

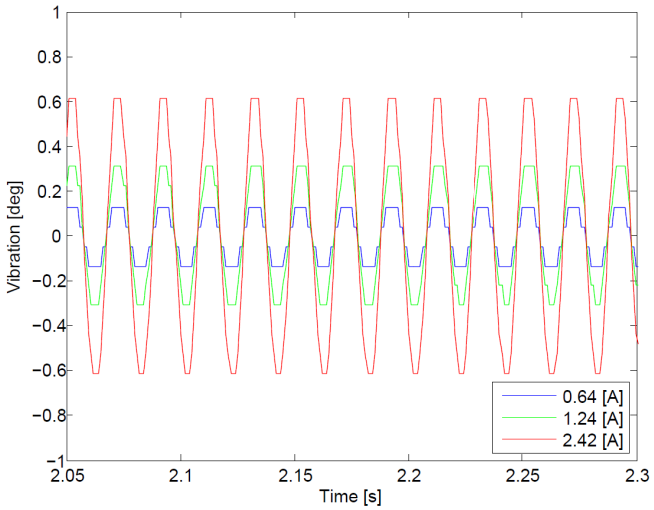

Fig. 3 - Rotor vibrations as a function of current

The vibrations appear as a sine wave with the grid frequency and the amplitude proportional to the motor current. Therefore, the rotor angle during the steady state charging operation can be expressed as

$$\theta(t) = \theta_o + A_\theta \cdot sin\,(2\pi f t + \theta_d) \qquad (9)$$

where A_θ is the vibration amplitude for the given current value. Combining the equations (3) - (5), (8) and (9), the maximum theoretical voltage disturbance due to rotor vibrations is obtained as

$$\hat{v}_{vib} = 2\pi f A_\theta \hat{I}_{ph} p L_{var} \qquad (10)$$

where $\hat{I}_{ph}$ is the phase current amplitude. This equation describes the worst case scenario in which the peak of the phase current occurs at the instance the rotor is in a position where the movement will cause the greatest inductance change ($L(\theta_r) = L_{mean}$). The actual instantaneous voltage disturbance will always be lower or equal. Maximum voltage disturbance for the used lab prototype has been evaluated as 1.05 V at the nameplate current of 4.1 A, which is less than 0.33% of the grid voltage and therefore can be neglected.

During the test the rotor was not mechanically loaded. In vehicle charging applications the rotor will be loaded by the weight of the vehicle, meaning that the actual vibrations will be partially or completely attenuated.

B. Power converter

Control of a PMSM in drive applications is done through an inverter. An inverter creates frequency and amplitude controllable AC voltages from the DC link voltage by applying sequences of fast switching voltage pulses at the converter output, which is connected to the machine terminals. By controlling the pulse durations, voltage waveform and RMS value can be controlled to follow the given reference. In drive applications, inverter gate pulses are given in such a manner that sinusoidal currents are produced in machine windings. Gate pulse calculation methods are called modulation techniques.

The same process can be reversed and an existing inverter can be used to rectify the input currents. Inverter and rectifier essentially share the same topology and it is only a matter of the control algorithm and power flow direction to determine whether they act as one or the other. Some converter implementations however, such as those with diodes in series with the switches, do not allow a bi-directional power flow. Therefore, a converter model has to be carefully selected. For this paper a two-level, three phase converter is chosen as shown in Fig. 1, which is the most simple and most widely used topology.

Applying no gate pulses to this converter makes it act like a six pulse diode rectifier due to anti-parallel diodes. This means the minimum DC link voltage is equal to the rectified voltage when the power factor is close to one. Normal operating mode delivers voltages above that level and in case a battery voltage is lower, the charging current cannot be controlled. A simplified single phase model of a converter represented as a controllable voltage source and machine windings as an inductor is shown in Fig. 4 (a). The vector diagram for the normal (boost) operating mode is shown in Fig. 4 (b). It can clearly be seen that it is not possible to achieve voltages below the grid voltage when operating at a unity power factor. However, by adding the reactive current component as shown in Fig. 4 (c), the rectified voltage can be reduced below the peak of the grid voltage. This is the basic operating principle of the voltage suppression mode.

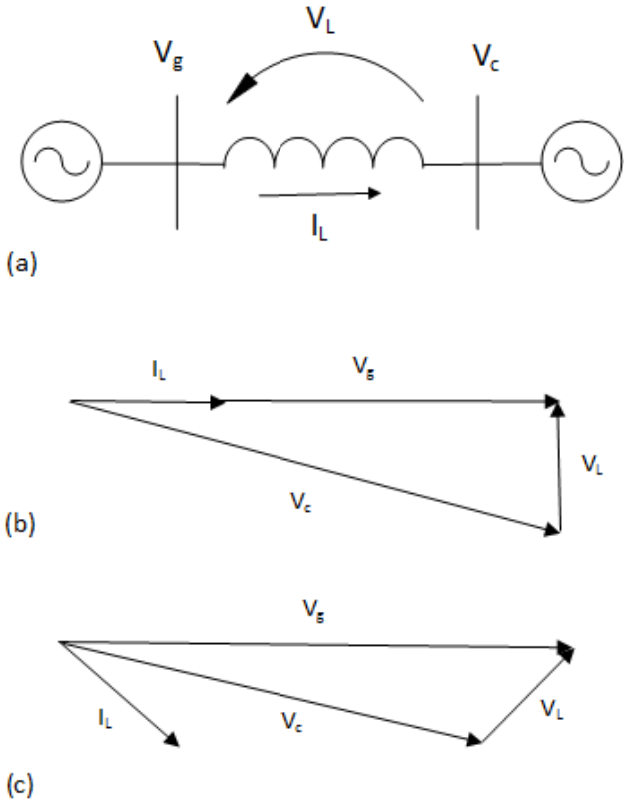

Fig. 4 - Single phase model of a converter as a controllable voltage source and vector diagrams for the boost and voltage suppression modes

III. CONTROL ALGORITHM

A. Space Vector Modulation

Space vector modulation technique has been selected for the active rectifier control. SVM has the advantage of producing the smallest current ripple, thus the emitted acoustic noise is the weakest [5]. Simultaneous control of all three phases is achieved using only two parameters - angle and amplitude.

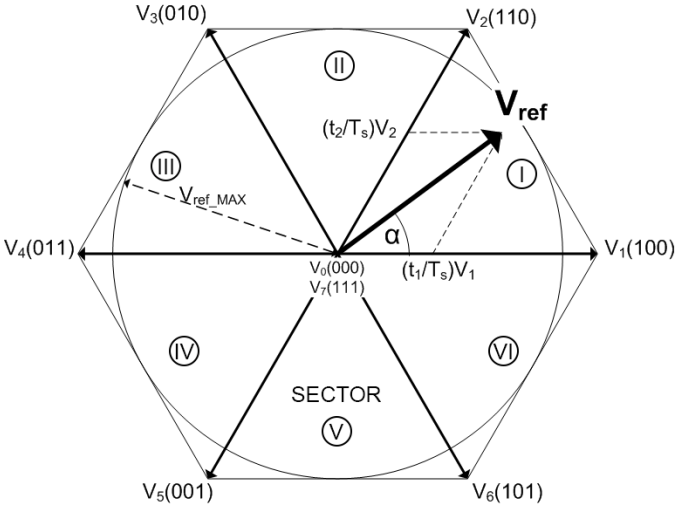

Fig. 5 - Representation of the reference voltage vector in the SVM plane

Graphical representation of space vectors in a complex plane is shown in Fig. 5. The selected converter topology allows a total of eight vectors corresponding to the state of switches (0 - inactive, 1 - active) and each vector can be represented by a binary 3-digit sequence. Six of them are active, while two of them (000 and 111) are zero vectors.

Any arbitrary reference vector $\vec{v}_{ref}$ with an amplitude V_{ref} and angle α can be constructed using the two neighboring vectors and null-vectors. Depending on the position and amplitude of the given reference vector, duty periods for the neighboring vectors are calculated using

$$d_1 = \frac{2}{\sqrt{3}} \frac{V_{ref}}{V_{max}} sin\left(\frac{\pi}{3} - \alpha\right) \quad (11)$$

$$d_2 = \frac{2}{\sqrt{3}} \frac{V_{ref}}{V_{max}} sin\,(\alpha) \quad (12)$$

$$d_0 = 1 - d_1 - d_2 \quad (13)$$

All the duty cycles are non-negative numbers less or equal to 1.

B. Boost rectifier mode

Batteries should be charged with constant current in order to maximize their lifetime. Therefore the algorithm is developed to follow the current reference. As the battery resistance is variable and dependent on the current state of charge, feedback current control has to be implemented.

Since the dynamics of battery charging are low (over a longer period of time at the same current applied), fast dynamic response is not a requirement for this system. It is however important to keep the overshoot within certain tolerance limits as the violation might trigger protection devices or damage the battery in the worst case.

In standard active rectifier applications the sinusoidal grid voltages can be converted to DC values using the rotating reference frame (RRF) transformation, also known as Clark-Park transformation. This transformation allows simple reference tracking using PI regulators. However, due to system disbalance, the dq current values are not pure DC anymore and an inverse sequence disturbance component twice the grid frequency will appear at the output [6]. The higher the amount of system disbalance, the stronger will the component be.

To ensure proper grid synchronization and compatibility with different frequencies, Synchronous Frame Phase Locked Loop (SF-PLL) [7] subsystem is implemented. Grid angle is obtained from the grid voltage measurements as they form a symmetrical system and contain less noise than the grid currents.

Block scheme of the boost mode control system is shown in Fig. 6. It consist of an inner voltage control loop and an outer current control loop. To avoid interference between the loops, the outer loop has around 10 times lower bandwidth than the inner loop. The space vector is synthesized from the vd1 and vq1 signals which are converted to the Static Reference Frame (SRF) using the obtained grid angle and fed to the space vector modulator to generate the converter gate pulses.

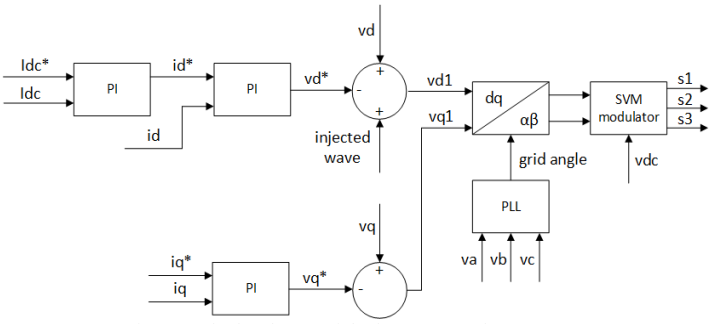

Fig. 6 – Block scheme of the boost control system

In the normal (boost) operation mode the DC link current value is controlled using the id current reference command while the iq is set to zero for the converter to operate at unity power factor. However, as stated before, due to system disbalance a 100 Hz ripple component will appear at the output. To compensate for the disturbance, a sine wave of adjustable amplitude and phase is injected to the d-axis voltage command.

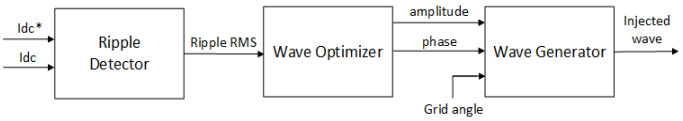

Fig. 7 – Block scheme of the wave compensation controller

The optimal sine wave amplitude and phase are dependent on the current reference, so they need to be dynamically changed. To achieve best transient performance, it is possible to determine the optimal values for each of the references and

implement them in a lookup table. However, as stated before, since the fast dynamic performance is not a requirement for the system, a generic wave compensation controller has been developed and its block diagram is shown in Fig. 7.

First, the ripple detector obtains the current ripple envelope. DC link current mean value is calculated and subtracted from the measured value. This extracts the ripple as an AC signal. Further processing is done and RMS value is calculated. This gives the ripple envelope which is fed to the wave optimizer.

The wave optimizer varies the amplitude and phase parameters of the injected wave utilizing the bisection method to determine the optimum and continues doing so until the convergence criteria has been fulfilled. If the reference value is changed, the ripple increase will be detected and the process will restart. Amplitude and phase values are fed to the wave generator which generates the compensation signal at twice the grid frequency.

The ripple reduction algorithm was simulated in Plecs and shown in Fig. 8. The machine parameters used were the same as for the lab prototype. The DC link reference current was 1 A and the battery was modeled as a 760 Ω resistor. The DC link capacitor was set to 5 µF.

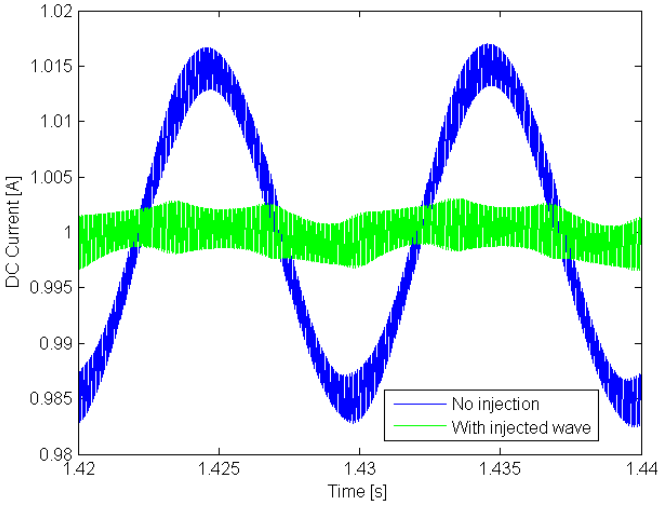

Fig. 8 - Current ripple reduction using the wave injection method

The uncompensated response has a significant 100 Hz ripple component with the amplitude of 1.7 % of the reference value. Compensating with the wave injection method the ripple amplitude was reduced below 0.3 % in steady state.

C. *Voltage suppression mode*

As stated in the introduction, there might be a need to deliver voltages below the diode bridge voltage to charge depleted batteries. From the Fig. 4 (c) it is visible that this can be done by lowering the power factor and increasing the reactive power consumption.

The block scheme of the voltage suppression mode control system is shown in Fig. 9. The main difference between the boost control system is that the outer control loop output is connected to both the id and iq controllers so that the power factor can be adjusted.

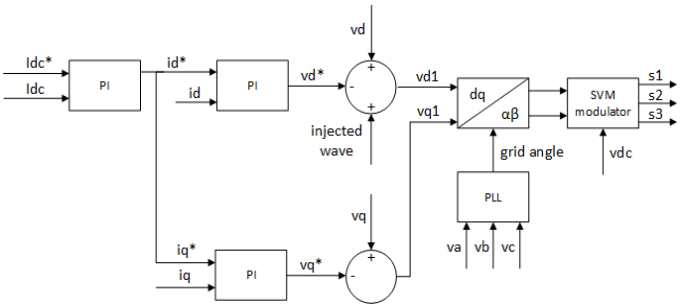

Fig. 9 - Block scheme of the voltage suppression mode control system

Since the controller is not operating at a unity power factor anymore, higher order harmonics appear at the output making it more difficult to compensate using the wave injection method. The lower the current reference, the higher the THD as the power factor decreases. This means that the compensation wave should contain several higher order harmonics. The more harmonics are included the better the compensation, but also the higher the wave optimizer complexity.

The injected wave compensation is done in the similar manner as in the boost mode – by injecting the compensation wave to the vd voltage reference. Even though the iq reference is dynamic in this case, due to the tendency to keep the power factor as high as possible, vq1 is significantly lower than vd1 and therefore compensating for both values would increase the complexity of the system and potentially cause interference between the injected wave controllers while not having a significant effect on the current ripple reduction.

D. *Mode selection*

There are three possible operation modes for this system – boost, voltage suppression and passive.

Passive mode is achieved by not giving any gate pulses to the rectifier and having all of the switches open. The conduction is done solely through the anti-parallel diodes and therefore the converter acts like a diode rectifier. The peak of the open circuit DC voltage is given by

$$\hat{V}_{dc} = \sqrt{6}\, V_{ph} \tag{14}$$

where V_{ph} is the RMS value of the grid phase voltage. This value is used to select between the boost and voltage suppression mode. The selection is based on the comparison between the desired output voltage and the diode bridge voltage. The desired output voltage is calculated using

$$V_{dc,ref} = I_{dc,ref} \cdot \frac{V_{dc,meas}}{I_{dc,meas}} \tag{15}$$

If the value obtained by equation (15) is higher than the one of equation (14), boost mode is selected, otherwise voltage suppression.

Equation (15) calculates the desired output voltage by multiplying the current reference value with the calculated load resistance. This is required as the battery resistance is variable and dependent on the current state of charge. There might be a concern that a mode selection error will occur in situations a step reference change is applied to the controller due to the fact the battery resistance changes over time, so the calculated

resistance at the instance of a reference change might be different than the actual resistance by the time the reference is reached. However, since the dynamics of battery resistance are a lot slower than the current controller, the battery resistance can be considered constant within the transient period and therefore no such error can occur.

IV. Experimental Validation

The algorithm was experimentally validated using a downscale setup. The 2.2 kW PMSM used had parameters as stated in section II.A and was connected to a 5.5 kW Danfoss FC302 VLT converter. The converter had an integrated 295 μF capacitor on the DC side. A 760 Ω resistor was used instead of an actual battery. The control algorithm was implemented in Simulink and deployed on a dSpace setup.

The boost mode test is shown in Fig. 10. Due to the large capacitor a converter had, the current waveform was already smoothened. However, using a wave injection the ripple was still reduced from 0.68 to 0.58 V RMS (0.083% to 0.071%), proving the concept works. Further tests should be carried out on a converter with a smaller DC link capacitor.

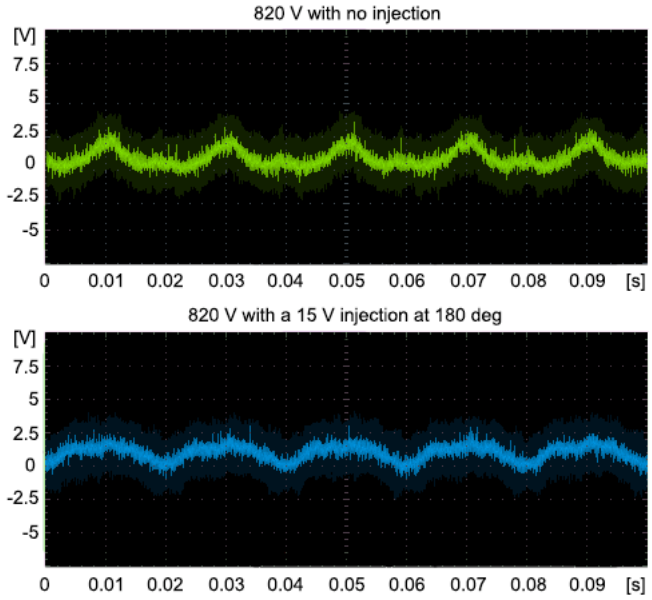

Fig. 10 - Boost mode test with the voltage DC component taken out for easier ripple visualization, upper plot shows the uncompensated response while the bottom response is compensated

Voltage suppression mode test is shown in Fig. 11. Due to the limited timeframe, a compensation was performed using only a 100 Hz sine wave instead of a complex wave consisting of first several higher order harmonics. The ripple was reduced from 3.48 to 1.68 V RMS (0.75% to 0.36%) proving the concept valid and further compensation could be achieved by taking into account higher order harmonics.

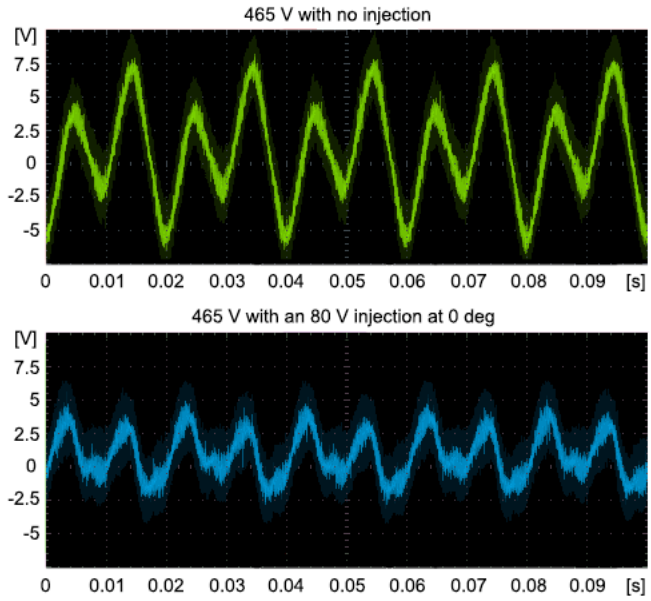

Fig. 11 - Voltage suppression mode test, upper plot shows the uncompensated response while the bottom response is compensated

V. Conclusion

In this paper a way of controlling an integrated vehicle charger using space vector modulation has been presented. The inverse sequence disturbance which appears due to disbalance in phase inductances was compensated for using the wave injection method. The effect of rotor vibrations on voltage variations was measured and assessed to be negligible. A voltage suppression mode was introduced for charging depleted batteries. All the solutions have been simulated using Plecs and experimentally tested on a downscale prototype. The results prove the concept valid, but further work is required on compensation in the voltage suppression mode as the injected wave should contain higher order harmonics to reduce the current ripple further.

References

[1] International Cleantech Network, "New International Study: Electric Vehicles Ready to Enter the Market but Significant Barriers still block the Road," Copenhagen, 2011.

[2] C.-S. N. Shiau, C. Samaras, R. Hauffe and J. J. Michalek, "Impact of battery weight and charging patterns on the economic and environmental benefits of plug-in hybrid vehicles," *Energy Policy,* no. 37, pp. 2653-2663, 2009.

[3] T. Poulsen, H. E. Tjelum, C. Vadstrup and S. S. Quillo, "Experimental Evaluation of an Integrated Charger for EV's Using PMSM Windings as Boost Inductors," Aalborg University, Aalborg, Denmark, 2011.

[4] D.-G. Woo, G.-Y. Choe, J.-S. Kim, B.-K. Lee, J. Hur and G.-B. Kang, "Comparisson of Integrated Battery Chargers for Plugin Hybrid Electric Vehicles: Topology and Control," 2011.

[5] A. Hava, R. Kerkman and T. Lipo, "Simple Analytical and Graphical Tools for Carrier Based PWM Methods," 1999.

[6] C. Jacobina, M. Correa, R. Pinheiro, E. da Silva and A. Lima, "Modeling and Control of Unbalanced Three-Phase Systems Containing PWM Converters," 1999.

[7] X.-Q. Guo, W.-Y. Wu and H.-R. Gu, "Phase locked loop and synchronization methods for grid-interfaced converters: A review," *Przegląd Elektrotechniczny (Electrical Review),* 2011.